(The article starts in the next page.)

Unsupervised Polarimetric SAR Image Classification using $\mathcal{G}_p^0$ Mixture Model

Juan I. Fernández-Michelli, Martín Hurtado, *Member, IEEE,* Javier A. Areta, *Member, IEEE,* and Carlos H. Muravchik, *Member, IEEE*

***Abstract*—This letter proposes a polarimetric Synthetic Aperture Radar (SAR) image classification method based on the Expectation-Maximization (EM) algorithm. It is an unsupervised algorithm that determines the number of classes in the scene following a top-down strategy using a covariance based hipothesis test. A $\mathcal{G}_p^0$ mixture model is used to describe Multilook Complex (MLC) polarimetric data, and the proposed algorithm is tested in simulated and real datasets obtaining good results. The classification performance is evaluated by means of the overall accuracy and the *kappa* indices obtained from Montecarlo analysis. Finally, the results are compared to those obtained by other classic and recently developed classification algorithms.**

***Index Terms*—SAR images, Classification, Radar Signal Processing, $\mathcal{G}_p^0$ distribution, EM algorithm, Mixture Models.**

I. Introduction

The process of SAR data classification is heavily dependent on the model and algorithms employed. The classical Wishart distribution based on the complex Gaussian model of the scattering coefficients successfully describes homogeneous areas with fully developed speckle and no texture [1]. The well known unsupervised classification method presented in [2] is based on the mentioned distribution and uses H/α decomposition [3] as initialization. However, the increasing resolution of SAR sensors due to the continuous technology improvement causes the classical models no longer fit to the measured data. Therefore, more complex models have to be used to interpret the observations.

In this regard, Frery et al. developed the $\mathcal{G}$ distribution family, which is capable of describing highly heterogeneous data [4]. However, the versatility of the $\mathcal{G}$ model has the complexity of its parameter estimation as counterpart. In [5], the authors proposed a mixture of $\mathcal{G}_p^0$ densities and the SEM (Stochastic Expectation Maximization) algorithm to classify PolSAR data, using the method of moments to estimate the parameters. In [6], the work presented in [5] was extended using different initializations. In both algorithms the number of classes in the dataset must be informed which establishes a semi-supervised approach. More recently, in [7] the authors proposed an automatic segmentation algorithm based on the $\mathcal{U}_d$-distribution and Markov Random Fields (MRF) to model the pixel's context information. The $\mathcal{U}_d$-distribution includes the $\mathcal{G}_p^0$ model as an asymptotic case but due to its complicated probability density function a close-form maximum-likelihood estimation solution does not exist [8], so the method of matrix log-cumulants was used in [7] to estimate its parameters.

In this work a classification algorithm based on the EM method and $\mathcal{G}_p^0$ mixture model is proposed. It is an unsupervised algorithm which only needs the equivalent number of looks as initial information. A Wishart statistic test provides the number and the structure of the classes in the image, and then the parameters of each class are estimated using the EM method. Instead of using moments or cumulants to estimate the parameters, the classification is performed using the maximum-likelihood estimates. In order to simplify the estimation process, the pixel labels are considered independent. The information of the pixel neighborhood is simply considered outside the EM loop using a mode filter. This is computationally less expensive than the MRF approach and yet produces good enough results.

Since the same data model and EM based approach as in [5] are used herein, the present work can be considered as its improved unsupervised extension that provides the MLE estimates of the model parameters. In [9] a semi-supervised version was presented, which is the base of the more complete version presented here. The paper proceeds as follows. In Section II the $\mathcal{G}_p^0$ mixture model used for PolSAR data is explained. In Section III, the five stages of the proposed algorithm are developed, and Sections IV and V present the results for simulated and real data respectively. The classification performance is evaluated in terms of the overall accuracy, the *kappa* statistic and computational cost. Finally, the conclusions are presented in Section VI.

II. Data Model

Polarimetric SAR data is built from radar return, which is related to the dielectric properties of the surface. The polarimetric data of a monostatic SAR are formed by a complex vector $\mathbf{z} = [s_{hh}\ \sqrt{2}s_{hv}\ s_{vv}]$, where hh, hv, vv are the polarization channels [10, p.65]. In homogeneous areas the scattering vector $\mathbf{z}$ is described by a complex circular Gaussian distribution. The asociated multilook complex data (MLC) defined as $\mathbf{Z} = \sum \mathbf{z}\mathbf{z}^H/n$ follow a Wishart distribution $\mathcal{W}_{\mathbb{C}}(\mathbf{C}, n)$, where $\mathbf{C} = \mathcal{E}\{\mathbf{z}\mathbf{z}^H\}$ is the covariance matrix, n is the number of looks, $(\cdot)^H$ denotes conjugate transpose and $\mathcal{E}\{\cdot\}$ denotes the expectation operator.

In non-homogeneous areas, the scattering vector deviates from the Gaussian statistic. Each fully polarimetric data point (pixel) $\mathbf{Z}$ can be described as the product of two stochastic variables $\mathbf{Z} = x\mathbf{Y}$, where $x \in \mathbb{R}^+$ describes the backscatter from the terrain and $\mathbf{Y} \in \mathbb{C}^{3\times 3}$ describes the speckle. In this work the $\mathcal{G}_p^0$ model is used. It was proposed in [11]

and it can successfully describe homogeneous, heterogeneous and extremely heterogeneous targets. In this context x is Inverse Gamma distributed with shape parameter $-\alpha$ and scale parameter γ: $x \sim \Gamma^{-1}(-\alpha, \gamma)$. $\mathbf{Y}$ obeys a Wishart distribution $\mathcal{W}_{\mathbb{C}}(\mathbf{C}, n)$, where n is the number of looks and $\mathbf{C}$ is the covariance matrix of the SAR return. The $\mathcal{G}_p^0$ density function for $\mathbf{Z}$ results:

$$f(\mathbf{Z};\boldsymbol{\theta}) = \frac{n^{nd}|\mathbf{Z}|^{n-d}\Gamma(dn-\alpha)}{h(n,d)|\mathbf{C}|^n\Gamma(-\alpha)(\gamma)^\alpha}(n\text{Tr}(\mathbf{C}^{-1}\mathbf{Z})+\gamma)^{\alpha-dn} \quad (1)$$

where $\boldsymbol{\theta} = (\alpha, \gamma, \mathbf{C}, n)$[1], $h(n,d) = \pi^{d(d-1)/2}\Gamma(n)\dots\Gamma(n-d+1)$ and $d = 3$ is the number of polarizations. The parameter $\alpha < 0$ is directly related with the rugosity of the terrain and $\mathbf{C}$ describes its polarimetric characteristics. $\text{Tr}(\cdot)$ and $|.|$ are the trace and determinant, respectively.

A. Mixture Model

Each pixel is modeled by a finite mixture of $\mathcal{G}_p^0$ densities:

$$f(\mathbf{Z}, \boldsymbol{\Theta}) = \sum_{j=1}^{K} \omega_j f_j(\mathbf{Z};\boldsymbol{\theta}_j), \quad (2)$$

where K represent the number of classes that compose the SAR return and f_j is the density given in (1). Each class is described by a set of parameters $\boldsymbol{\theta}_j = (\alpha_j, \gamma_j, \mathbf{C}_j, n_j)$. The coefficients w_j indicate the proportion of the jth component in the mixture, subject to the restrictions $\sum_{j=1}^{K}\omega_j = 1$ and $\omega_j \geq 0$, $j = 1\dots K$. The vector parameter of the mixture is $\boldsymbol{\Theta} = (\omega_1, \dots, \omega_K, \boldsymbol{\theta}_1, \dots, \boldsymbol{\theta}_K)$.

III. Algorithm structure

The proposed algorithm follows a top-down strategy, composed of five stages: initialization, split-and-merge, estimation, classification and smoothing. It begins with a unique class and iteratively divides the dataset into more classes as it finds evidence of more complex structures within each class. This stage provides a suitable initialization to the EM algorithm which computes the parameter estimates of the mixture model and the labeled image. Finally, a simple non-linear mode filter is applied to obtain the final image.

After a trivial initialization, the Split-and-Merge stage is performed to determine K, the number of classes in the dataset. It is based on the Wishart covariance matrices test [12] and the Wishart classifier [2]. This stage also provides the initialization (labeled pixels) for the next stage. The estimation stage applies the EM algorithm to the $\mathcal{G}_p^0$ mixture model to estimate the parameter vector $\boldsymbol{\Theta} = (\omega_1, \dots, \omega_K, \boldsymbol{\theta}_1, \dots, \boldsymbol{\theta}_K)$. In the next stage the algorithm performs a Maximum A Posteriori (MAP) classification of every pixel in the dataset based on the estimated parameters $\boldsymbol{\theta}_j$. Finally, a non-linear filter (mode filter) is applied on the labeled data to smooth the resulting image. In the following sections the details of each stage of the algorithm are provided.

[1]It is worth noting that, since in the multiplicative model x has unitary mean, it is possible to eliminate γ from the $\mathcal{G}_p^0$ expression as indicated in [11]. In this letter γ is preserved maintaining the unitary mean, without loss of generality.

A. Initilization

As a very undemanding initialization, every pixel in the dataset is assigned to a unique initial class. This is the first step of the top-down strategy performed in the following stage to capture the classes structure of the dataset.

B. Split and Merge

In this stage the number of classes K, a class-partition data P_K and set of covariance matrices $\{\mathbf{M}\} = \{\mathbf{M}_1, \dots, \mathbf{M}_K\}$ describing each class center are obtained. The partition P_K and $\{\mathbf{M}\}$ will be used as the initialization for the next stage.

This stage proceeds iteratively. Assuming there are K_L classes and a partition P_{K_L} at Lth iteration, the randomly initialized Wishart classifier is applied to the pixels in each class to identify two subclasses. After convergence is reached, there are two covariance matrices $\mathbf{M}_{i1}$ and $\mathbf{M}_{i2}$ as the estimated subclass centers for each class $\mathcal{C}_i$. It must be determined whether this two subclasses are sufficiently separated as to consider them two distinct clusters. In order to do that, the Wishart covariance matrix test developed in [12] is used as the cluster separation measure. The test considers the null hypotheses $H_0 : \mathbf{M}_{i1} = \mathbf{M}_{i2}$ against the alternative $H_1 : \mathbf{M}_{i1} \neq \mathbf{M}_{i2}$. Under H_0 the loglikelihood-ratio test becomes

$$\log Q = n(2d\log 2 + \log|\mathbf{M}_{i1}| + \log|\mathbf{M}_{i2}| - 2\log|\mathbf{M}_{i1}+\mathbf{M}_{i2}|). \quad (3)$$

The probability of z being smaller than $-2\rho\log Q$ is

$$P\{-2\rho\log Q \leq z\} = P\{\chi^2(d^2) \leq z\} + wP\{\chi^2(d^2+4) \leq z\} - wP\{\chi^2(d^2) \leq z\} \quad (4)$$

where $\rho = 1 - 17/12n$ and $w = -d^2(1-1/\rho)^2/4 + 7d^2(d^2-1)/(96n^2\rho^2)$ [12]. Given a probability of false alarm (PFA), a threshold $\Lambda | P\{-2\rho\log Q \leq \Lambda\} = 1 - \text{PFA}$ is computed using (4) and compared with $Q' = -2\rho\log Q$. If $Q' \leq \Lambda$ H_0 is accepted and the class is not divided. If $Q' > \Lambda$, H_0 is rejected, meaning that there is enough evidence to assume that the matrices describe different classes. Therefore, the class is divided according to the Wishart classification and $\mathbf{M}_{i1}$, $\mathbf{M}_{i2}$ are the new class centers.

After this split process is performed for the K_L classes, a merging process is needed because subclasses belonging to different classes were not tested, and it is possible that they belong to the same class. The expression (3) is computed for all matrices resulting from the split process, $\mathbf{M}_{ik}$, $\mathbf{M}_{jr}$, $i, j = 1\dots K_L, i \neq j;\ k, r = \{1, 2\}$. Using the same PFA, those test values smaller than Λ indicate acceptance of H_0, i.e. they belong to the same class and should be merged. The minimum of those values (corresponding to most similar matrices) indicates that their respective classes have to be merged: their pixels are relabeled with a unique value and a new class center is calculated as the mean of the two involved subclass centers. After this split and merge process, there are K_{L+1} classes, with $K_{L+1} \in [K_L, 2K_L]$. In the next iteration $L+1$, the process is repeated for K_{L+1} classes. It stops when $K_M = K_{M+1} = K$ and there were no merged classes in the Mth iteration.

This simple procedure allows to identify the class structure of the dataset using the number of looks as the only required information. The PFA acts as adjusting variable, setting the sensibility of the process to differentiate classes.

C. Estimation

In order to estimate the vector parameter $\mathbf{\Theta}$ of the mixture model (2), the EM algorithm [13] is applied with K classes, P_K partition and class centers $\{\mathbf{M}\}$ as initialization. Avoiding the details of the calculation, the lth EM iteration expressions are:

Expectation step:

$$\gamma_{ij}^{(l)} = \frac{\omega_j^{(l-1)} f_j(\mathbf{Z}_i, \boldsymbol{\theta}_j^{(l-1)})}{\sum_{r=1}^{K} \omega_r^{(l-1)} f_r(\mathbf{Z}_i, \boldsymbol{\theta}_r^{(l-1)})} \tag{5}$$

Maximization step:

$$\omega_j^{(l)} = \frac{\sum_{i=1}^{N} \gamma_{ij}^{(l)}}{N} = \frac{N_j^{(l)}}{N} \tag{6}$$

$$\mathbf{C}_j^{(l)} = -\nu_j \sum_{i=1}^{N} \gamma_{ij}^{(l)} \frac{\mathbf{Z}_i}{n\mathrm{Tr}(\mathbf{C}_j^{(l)^{-1}} \mathbf{Z}_i) + \gamma_j} \tag{7}$$

$$\begin{aligned} \mathcal{L} =& N_j^{(l)} \log(\Gamma(nd - \alpha_j)) \\ & - N_j^{(l)} \log(\Gamma(-\alpha_j)) - N_j^{(l)} \alpha_j \log(\gamma_j) \\ & + \sum_{i=1}^{N} \gamma_{ij}^{(l)} (\alpha_j - nd) \log(n(\mathrm{Tr}(\mathbf{C}_j^{-1} \mathbf{Z}_i)) + \gamma_j) \end{aligned} \tag{8}$$

where $\nu_j = (nd - \alpha_j)/N_j^{(l)}$, $N_j^{(l)} = \sum_i \gamma_{ij}$ and N is the total number of pixels.

The parameter $\gamma_{ij}^{(l)}$ in Eq. (5) computes the posterior probability of the i data point belonging to the jth class, at the lth iteration. Eq. (7) computes the covariance matrices of each class. $\mathcal{L}$ is an expression to be maximized with respect to α_j and γ_j. Because Eqs. (7) and (8) are not independent, the Expectation Conditional Maximization (ECM) method is used [14] that consists of maximizing each variable conditioned to the others, i.e constraining the parameters space in each maximization where the collection of all constrains is such that the maximization is over the full parameter space. Therefore, first (7) is solved with fixed α_j and γ_j, and then $\mathcal{L}$ is maximized with the obtained $\mathbf{C}_j$. Both procedures are performed numerically for every iteration of the EM algorithm.

The solution for the expression (7) requires deeper explanation. It is a trascendental equation with no analytical solution. To solve it, the principle derived in [15] is used. $\mathbf{C}_j^{(l)}$ is found recursively as:

$$\mathbf{C}_j^{(t+1)} = -\nu_j \sum_{i=1}^{N} \gamma_{ij}^{(l)} \frac{\mathbf{Z}_i}{n\mathrm{Tr}(\mathbf{C}_j^{-1^{(t)}} \mathbf{Z}_i) + \gamma_j} \tag{9}$$

initializing with the covariance matrix computed in the previous EM iteration: $\mathbf{C}_j{}^{(t=0)} = \mathbf{C}_j{}^{(l-1)}$. Although the convergence of the proposed recursion is not demonstrated in this work, it was extensively tested and in all the cases converged to the correct value. The computation stops when

$$\epsilon = \frac{\|\mathbf{C}_j^{(t+1)} - \mathbf{C}_j^{(t)}\|_F}{\|\mathbf{C}_j^{(t)}\|_F} \tag{10}$$

becomes smaller than a predefined value. $\|\cdot\|_F$ represents the Frobenius norm. When convergence is reached $\mathbf{C}_j^{(t)} \approx \mathbf{C}_j^{(t+1)} = \mathbf{C}_j^{(l)}$.

After the EM algorithm achieves the convergence, the vector estimate $\hat{\mathbf{\Theta}}$ that fully describes the mixture model (2) is known. Because the complete estimation process comprises two nested iterative algorithms (EM and covariance estimation), it can take too long if the whole dataset is used. Therefore a representative subset of data can be used to speed up the estimation. The algorithm was tested with data subsets formed by randomly sampling the original data up to a factor of 0.6 (60% of the original dataset) with no appreciable degradation in the estimation results.

D. Classification

In this stage a MAP classification is performed. Once the estimation stage is completed, all the classes in the mixture are identified by the estimated parameters. Every original data point $\mathbf{Z}_i$ is then assigned to the class with the greatest likelihood, providing a labeled image that represents the classification result:

$$\mathcal{C}_j \leftarrow \mathbf{Z}_i \ , \ j = \underset{j}{\mathrm{argmax}} \, f_j(\mathbf{Z}_i, \boldsymbol{\theta}_j), \forall i, j.$$

E. Smoothing

After MAP classification, the labeled image may appear noisy, with groups of pixels with different labels to their surrounding neighbors labels. This effect is a known issue of MLE based algorithms, when no pixel neighborhood information is used in the estimation process. Hence, a nonlinear 3×3 window size mode filter is applied to the labeled data in order to model spatial correlation, thus improving visualization of the results.

IV. Performance with Simulated Data

In order to evaluate the performance of the algorithm, a Montecarlo analysis was performed. Several SAR images were simulated with four classes using the mixture model (2). Each class is described with a $\mathcal{G}_p^0$ density and every one of them contributes to the mixture equally ($\omega_j = 1/4, j = 1 \ldots 4$). Every class realization was generated according to the procedure suggested in [5] using the multiplicative model described in Section II with the covariance matrices $\mathbf{C}_j = \mathrm{Toepl}([1 \ \rho_j \ \rho_j^2])$, where $\rho_1 = 0.8003 + j0.1419$ (cyan), $\rho_2 = 0.4715 - j0.1927$ (red), $\rho_3 = 0.1576 - j0.9706$ (yellow) and $\rho 4 = -0.4404 - j0.1645$ (blue). This values were proposed in [16] to generate polarimetric SAR matrices. The expression $\mathrm{Toepl}([a \ b \ c])$ indicates the Hermitian Toeplitz matrix with first column $[a \ b \ c]$. In every Montecarlo configuration a four classes SAR image was simulated with covariances $\mathbf{C}_j$, and α and n taken from the lists $\alpha =$

$\{-1.5, -2, -2.5, -3, -3.5, -4, -4.5, -5, -5.5, -6, -10\}$, $n = \{5, 7, 9, 15, 25\}$. Fifty datasets were generated for each configuration, giving a total of 2750 Montecarlo runs. Fig. 1(a) shows the span image of a Montecarlo realization. Each zone consisting of 100×100 pixels is assigned to a class of the simulated mixture model.

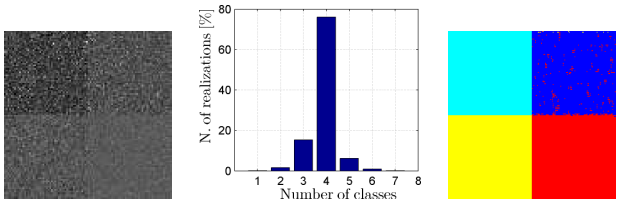

Figure 1. (a): Span image of one Montecarlo realization (simulated terrain). (b): Histogram of the detected number of classes on 2750 runs. (c): Classification result example for simulated data.

The proposed algorithm was applied to every Montecarlo realization. Two different aspects of the algorithm were tested: its ability to identify the correct number of classes and the accuracy of the classification. The former was evaluated by counting the resulting classifications which identified four classes. In order to evaluate the accuracy, the confusion matrix and the associated *kappa* index [17] were computed for each classification in which 4 classes were identified. The average of the *kappa* values is a measure of the accuracy of the algorithm. Fig. 1(b) shows the Montecarlo results for the identified number of classes, showing low dispersion around the correct value and Fig. 1(c) shows a representative classification (resulting from a single Montecarlo realization). The performance indices of the complete Montecarlo analysis results in an average overall accuracy of **0.9967** and an average *kappa* index of **0.9958**, showing an excellent level of agreement with the simulated terrain.

V. Performance with Real Data

In the present section the proposed algorithm is tested with real SAR MLC data, corresponding to an AIRSAR 450×500 pixels image of the San Francisco area[2]. Fig. 2 shows the scene in RGB false color and the defined control zones, identifying the different classes in the image: sea, vegetation, urban and coast. The first three classes are visually distinguishable, while the coast class is hidden, but it has been identified in previous works [10]. These zones are used as ground truth to evaluate the performance using the confusion matrix.

In order to test the consistency and accuracy, the proposed algorithm was applied 40 times to the real dataset, with PFA=0.05 and n=3.4[3]. The confusion matrix and related indices were computed for every classification result and the averaged overall accuracy and *kappa* values were computed to measure the performance.

In addition, three different algorithms were implemented and tested with the same real dataset to compare the performances: the classic Wishart classifier (WC) [2] with random initialization, the recently developed Spectral Clustering algorithm (SC) described in [18] and the Horta's classification algorithm (HC) with percentile initialization [5]. Since these algorithms can not determine the number of classes, the correct number of four classes was informed to them. In the case of the SC algorithm, it requieres a number of superpixels (N_{sp}) to perform the initial image segmentation and a width parameter (σ) to define the kernel function. These parameters were tuned to obtain the best classifications results for the dataset under study, which result in $N_{sp} = 500$ and $\sigma = 7$.

Figure 2. San Francisco image [R= hh, G= hv, B= vv]. Control zones: blue: sea, red: urban, green: vegetation, white: coast.

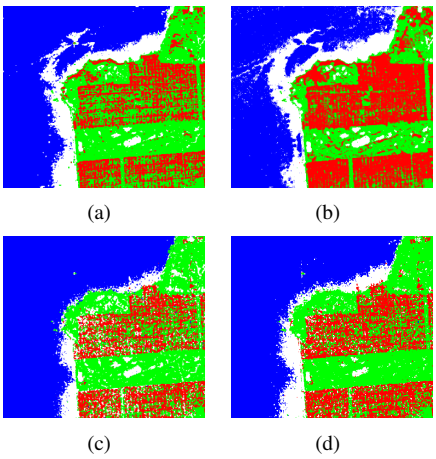

Figure 3. Classification results: (a) Wishart Classifier (WC). (b) Spectral Clustering (SC). (c) Horta's algorithm (HC). (d) Proposed algorithm.

The representative labeled images are shown in Fig. 3 for each algorithm. It can be observed that both WC and SC algorithms oversized the "coast" class, while the latter identifies the "urban" class more densely than the other algorithms. The resulting images from the proposed and HC algorithms are very similar because they are based on the same data model. However, the proposed algorithm identifies the "coast" and "urban" classes better than HC. Table I shows the performance average indices of the 40 classifications[4]. The proposed approach follows closely the performance of the SC algorithm; however, it must be remarked that SC requires fine tuning in order to reach acceptable results. In addition, the small difference is largely compensated with the much lower computational cost, which is three times smaller in terms of processing time. The WC and HC algorithms present even

[2]Available in https://earth.esa.int/web/polsarpro/airborne-data-sources

[3]This value was previously estimated in [6] using the same dataset.

[4]In the case of the SC algorithm, only the best classification was considered because that algorithm does not have any random stage. The classification result is completely determined once N_{sp}, σ and the input data are set.

smaller processing times, but their performance parameters are significantly worse. The experiments were made on a desktop PC with the following characteristics: O.S. Windows 7, CPU Intel Core i3 3.1GHz, RAM 8GB.

Table I
PERFORMANCE FOR REAL DATA

	Algorithm			
	WC	SC	HC	Proposed
accuracy	0.8426	0.8761	0.8292	0.8639
kappa	0.7597	0.8086	0.7382	0.7933
CPU time [sec]	336	9310	817	3091

VI. CONCLUSION

An unsupervised algorithm for polarimetric SAR data classification based on the $\mathcal{G}_p^0$ model was developed. The top-down approach of the Split-and-Merge stage provides the number of classes and a suitable initialization to the EM algorithm. Since it starts with a unique class for the whole image, it makes the classification insensitive to the initialization. In addition to the classification results, the proposed algorithm provides the MLE estimates of the mixture unlike the moments based estimates provided by [5] and [6], at the cost of a more computationally expensive M step.

The proposed algorithm was applied to simulated and real data. In the former case the Montecarlo analysis showed low dispersion in the identified number of classes, which validates the Split-and-Merge stage, and very accurate results in terms of average overall accuracy and *kappa* indices, which validates the Estimation and Classification stages. In the case of real data, the algorithm showed high consistency by identifying the reference zones in all the cases, with high accuracy in the classification results, comparable to those obtained by supervised state-of-the-art algorithms [19], [20].

Three additional classification algorithms were implemented for comparison purposes: the classic Wishart algorithm, Horta's algorithm, which uses the same data model, and a recently developed spectral clustering algorithm. The proposed algorithm showed a better performance considering the *kappa* index and processing time. In addition, unlike the competitors, it can determine the number of classes in a dataset without previous information.

The proposed algorithm has only the PFA as adjusting parameter, which set its sensitivity in the classes identification process. This is an additional advantage over the spectral clustering algorithm where N_{sp} and σ have to be set. Furthermore, the performance of the SP algorithm probed to be very sensitive to the kernel width σ, which has to be manually tuned for every new dataset.

The MATLAB code along with the required datasets to reproduce the results can be found at http://www.ieeexplore.org.

Future work will be centered in improving the Split-and-Merge stage. The Wishart classifier used to estimate the covariance matrices could be replaced by other less expensive methods. In addition, although it did not represent an issue in the present work, convergence of Eq. (7) has to be studied. A suitable alternative is to adapt the problem to fit the hypothesis of the work presented in [16] where convergence has been proved.

ACKNOWLEDGMENT

This work was supported by ANPCyT PICT 2014-1232, UNLP 11-I-209, CONICET and CICpBA.

REFERENCES

[1] V. Akbari, S. N. Anfinsen, A. P. Doulgeris, and T. Eltoft, "A change detector for polarimetric sar data based on the relaxed wishart distribution," in *2015 IEEE International Geoscience and Remote Sensing Symposium (IGARSS)*, July 2015, pp. 3806–3809.

[2] J. S. Lee, M. Grunes, T. Ainsworth, L.-J. Du, D. Schuler, and S.R.Cloude, "Unsupervised classification using polarimetric decomposition and the complex Wishart classifier," *IEEE Trans. Geosci. Remote Sens.*, vol. 37, no. 5, pp. 2249–2258, 1999.

[3] S. Cloude and E. Pottier, "An entropy based classification scheme for land applications of polarimetric SAR," *IEEE Trans. Geosci. Remote Sens.*, vol. 35, no. 1, pp. 68–78, Jan 1997.

[4] A. Frery, H.-J. Muller, C. Yanasse, and S. Sant'Anna, "A model for extremely heterogeneous clutter," *IEEE Trans. Geosci. Remote Sens.*, vol. 35, no. 3, pp. 648–659, May 1997.

[5] M. M. Horta, N. Mascarenhas, A. C. Frery, and A. Levada, "Clustering of fully polarimetric SAR data using finite Gp0 mixture model and SEM algorithm," in *Proc. 15th International Conf. on Systems, Signals and Image Processing (IWSSIP 2008)*, 2008, pp. 81–84.

[6] M. M. Horta, N. Mascarenhas, and A. C. Frery, "A comparison of clustering fully polarimetric SAR images using SEM algorithm and Gp0 mixture modelwith different initializations," in *Proc. 19th International Conf. on Pattern Recognition (ICPR 2008)*, 2008, pp. 1–4.

[7] A. P. Doulgeris, V. Akbari, and T. Eltoft, "Automatic polsar segmentation with the U-distribution and markov random fields," in *Synthetic Aperture Radar, 2012. EUSAR. 9th European Conf.*, April 2012, pp. 183–186.

[8] A. P. Doulgeris, "An automatic U-distribution and markov random field segmentation algorithm for polsar images," *IEEE Trans. Geosci. Remote Sens.*, vol. 53, no. 4, pp. 1819–1827, April 2015.

[9] J. I. Fernandez-Michelli, J. A. Areta, M. Hurtado, and C. H. Muravchik, "Polarimetric SAR image classification using EM method and Gp0 model," in *2015 XVI Workshop on Inf. Proc. and Control*, Oct 2015.

[10] J. S. Lee and E. Pottier, *Polarimetric Radar Imaging: from Basics to Applications*, ser. Optical science and Engineering. CRC Press, Taylor and Francis Group, 2009.

[11] C. C. Freitas, A. C. Frery, and A. H. Correia, "The polarimetric g distribution for SAR data analysis," *Environmetrics*, vol. 16, no. 1, pp. 13–31, 2005.

[12] K. Conradsen, A. A. Nielsen, J. Schou, and H. Skriver, "A test statistic in the complex wishart distribution and its application to change detection in polarimetric SAR data," *IEEE Trans. Geosci. Remote Sens.*, vol. 41, no. 1, pp. 4–19, January 2003.

[13] A. P. Dempster, N. M. Laird, and D. B. Rubin, "Maximum likelihood from incomplete data via the em algorithm," *Journal of the Royal Statistical Society. Series B*, vol. 39, no. 1, pp. 1–38, 1977.

[14] G. J. McLachlan and T. Krishnan, *The EM Algorithm and Extensions*, 2nd ed., ser. Series in Probability and Statistics. J. Wiley, 2008.

[15] E. Conte, A. De Maio, and G. Ricci, "Recursive estimation of the covariance matrix of a compound-Gaussian process and its application to adaptive CFAR detection," *IEEE Trans. Signal Process.*, vol. 50, no. 8, pp. 1908–1915, Aug 2002.

[16] P. Formont, J.-P. Ovarlez, and F. Pascal, "On the use of matrix information geometry for polarimetric SAR image classification," in *Matrix Information Geometry*, F. Nielsen and R. Bhatia, Eds. Springer Berlin Heidelberg, 2013, pp. 257–276.

[17] S. V. Stehman, "Selecting and interpreting measures of thematic classification accuracy," *Remote Sensing of Environment*, vol. 62, no. 1, pp. 77 – 89, 1997.

[18] H. Song, W. Yang, Y. Bai, and X. Xu, "Unsupervised classification of polarimetric SAR imagery using large-scale spectral clustering with spatial constraints," *International Journal of Remote Sensing*, vol. 36, no. 11, pp. 2816–2830, 2015.

[19] A. Zehtabian and H. Ghassemian, "Automatic object-based hyperspectral image classification using complex diffusions and a new distance metric," *IEEE Trans. Geosci. Remote Sens.*, vol. 54, no. 7, pp. 4106–4114, July 2016.

[20] P. Ghamisi, J. A. Benediktsson, G. Cavallaro, and A. Plaza, "Automatic framework for spectral spatial classification based on supervised feature extraction and morphological attribute profiles," *IEEE Journal of Selected Topics in Applied Earth Observations and Remote Sensing*, vol. 7, no. 6, pp. 2147–2160, June 2014.